The 2010 IEEE/RSJ International Conference on
Intelligent Robots and Systems
October 18-22, 2010, Taipei, Taiwan

Rover control based on an optimal torque distribution - Application to 6 motorized wheels passive rover

Ambroise Krebs, Fabian Risch, Thomas Thueer, Jérôme Maye, Cédric Pradalier and Roland Siegwart

Abstract— **The capability to overcome terrain irregularities or obstacles, named terrainability, is mostly dependant on the suspension mechanism of the rover and its control. For a given wheeled robot, the terrainability can be improved by using a sophisticated control, and is somewhat related to minimizing wheel slip. The proposed control method, named torque control, improves the rover terrainability by taking into account the whole mechanical structure. The rover model is based on the Newton-Euler equations and knowing the complete state of the mechanical structures allows us to compute the force distribution in the structure, and especially between the wheels and the ground. Thus, a set of torques maximizing the traction can be used to drive the rover. The torque control algorithm is presented in this paper, as well as tests showing its impact and improvement in terms of terrainability. Using the CRAB rover platform, we show that the torque control not only increases the climbing performance but also limits odometric errors and reduces the overall power consumption.**

I. Introduction

On the 26th of April 2005 (SOL 446[1]), one of the two Mars exploration rovers (MER) of NASA, Opportunity, got almost stuck in a sand dune in Meridiani Planum. On the 12th of May 2009 the other MER, Spirit, got trapped at his turn and was retasked as a "stationary research platform". These examples show how fatal wheel slip can be for autonomous rovers and how important it is to control an exploration rover as well as possible to lower the potential risks. Minimizing slip, or maximizing the rover traction is also related to the rover capability to negotiate the terrain irregularities named terrainability [1]. This rover property is influenced mostly by two aspects one can act upon; the kinematics of its suspension system and how well its actuators are controlled. The topic of optimal control for a rough-terrain rover lies in the main focus of the work presented here.

A. Related Work

For wheeled rough terrain robots, enhanced performances can be obtained by maximizing the traction [2]. This allows getting the maximum from a rover in terms of obstacle climbing capability or minimizes its risk of getting stuck. This method can also be formulated as minimizing slip, which also improves odometry, and therefore, has a double positive impact on the rover performance. In this sense, several algorithms have been proposed, such as [3]. In this case, the wheel velocities are synchronized in order to avoid them fighting each other. Although this approach is proven to be efficient, its impact is limited as it considers only the velocities of the wheels. In fact, this method as well as similar ones does not take into account the kinematics or the physical model of the rover and thus their results are expected to be limited in challenging terrain. [4] presents a control methodology which can minimize power consumption in relatively flat terrain and maximize traction in highly uneven terrains. As this work concerns the 2D case only, an extension to a 3D model was proposed in [5]. The resulting controller was then tested in simulation in [6] for the SOLERO [7] rover. Although this showed very good results in terms of slippage, this approach was unfortunately not implemented and tested on real hardware, mainly due to a lack of appropriate sensors. Finally, let us also mention [8] as other works which model the slippage according to the terrain to correct it. The approach is really efficient to reduce the rover slippage, but is complementary to our own and does not necessarily improve the terrainability.

B. Content

In the context of a pre-study for the European Space Agency (ESA) project Exomars [9], the development of a new robotic platform called CRAB [10], depicted in Fig. 1, offered a new opportunity to pursue the idea of implementing and testing this controller. This paper describes the required development of the CRAB rover, as well as the torque control impact. The following section gives an overview of the torque control. Section III presents briefly the CRAB and its model. The next section focuses on the sensors providing the state of the rover, and especially the CRAB's tactile wheels. Section V presents the results and a conclusion ends the paper.

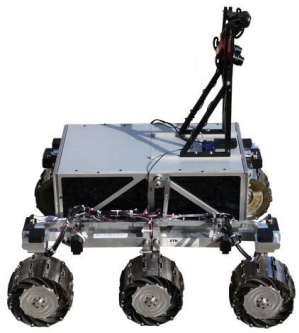

Fig. 1. CRAB rover with the tactile wheels.

This work was partially supported by ESA

All authors are with the Autonomous Systems Lab (ASL), Swiss Federal Institute of Technology Zürich (ETHZ), 8092 Zürich, Switzerland
name.surname@mavt.ethz.ch

[1]http://marsrovers.nasa.gov/mission/status_opportunityAll_2005.html#sol446

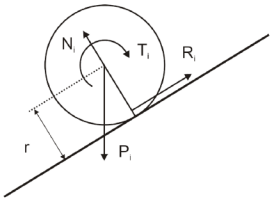

Fig. 2. Forces acting on the i^{th} wheel.

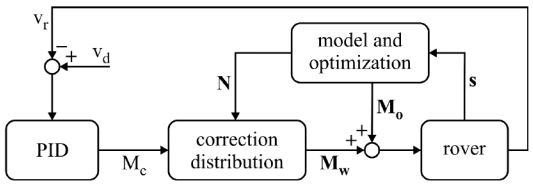

Fig. 3. Control scheme based on optimal torques and overlaid PID velocity regulator.

II. Torque Control Overview

The passive wheeled robots are mechanisms which have a single degree of freedom (DOF) and accordingly require a single actuator to be controlled. Nevertheless in the context of exploration in rough terrain, the robots can face very challenging terrain and in order to enhance their terrainability, all their wheels are motorized. This statement is true for the CRAB which, being equipped with six motorized wheels, is over-actuated.

A. Optimal Control

The fundamental idea of the controller consists of minimizing slip by efficiently distributing the torques on the wheels, using a static model. The more a wheel is loaded, the higher the torque applied can be before it slips. For this reason, the controller is referred to as torque control. Considering a rover's wheel as depicted in Fig. 2, the forces in action are the tangential, R_i, and normal, N_i, force, the load, P_i, and the motor torque, T_i. Note also that r represents the wheel radius. The tangential force is linked with the normal force as follow:

$$R_i = \mu N_i, \tag{1}$$

with μ being the friction coefficient. This equation is true whether the wheel slips or not, but if μ is smaller or equal to the static friction coefficient μ_0, the wheel does not slip:

$$\mu \leq \mu_0. \tag{2}$$

B. Torque Control

If a vehicle is moving on uneven terrain, the load on each wheel changes continuously and the maximum traction possible at each wheel varies accordingly. The torque control algorithm takes these state changes into account by estimating the load distribution based on a static model. Since the model is statically indeterminate due to the motorization of all wheels, an optimization algorithm is applied to find the set of motor torques that requires the least overall traction. It was shown in [5] that the least required friction result can be found using:

$$H = min\left(\sum_i (G_i - \overline{G})^2\right), \tag{3}$$

with

$$G_i = \frac{R_i}{N_i}. \tag{4}$$

Note that G_i is the required μ to avoid slippage and can be seen as a metric, with $\overline{G}$ its mean value. G_i is therefore different from μ, the actual friction coefficient. For over-actuated rover, such as the CRAB rover, an infinite number of set of torques allows to keep its static equilibrium. Among all these possible sets, eq. 3 determines the optimal set of torque minimizing the slippage risk.

C. Rover Motion

Since the torque control algorithm makes use of a static model, a velocity component has to be introduced in the control loop. The corresponding control scheme was introduced in [6] and is depicted in Fig. 3. In the inner loop the rover state, s, is used to update the static model and calculate the optimal torques, M_o. As no motion is generated, the outer loop is added to control the rover's velocity. The rover's actual velocity, v_r, is compared to the desired velocity, v_d, and the error is used to compute a correction torque, M_c. In order to comply with the objective of assigning torques according to the normal forces, N, on the wheels, a correction distribution is calculated in function of N to find the individual wheel correction torques, M_w, which are finally added to the optimal torques, M_o, and make the rover move at the desired speed.

In order to show the utility of a new control algorithm, it has to be compared to existing control. Therefore, the optimal torque algorithm is compared in this work to velocity control. Velocity control is supported by most hardware controllers, requires only little sensor information and no modeling. The velocities of all wheels are compared to the desired velocity and the errors are used in individual PID controllers to calculate the correction required to attain the commanded velocity.

III. Rover Breadboard: CRAB

The platform used for the tests is the CRAB rover. It is a six motorized wheels robot with a passive suspension system. The suspension system is composed of two symmetrical structures such as depicted in Fig. 4, one on each side of the rover. It makes use of parallel kinematic elements like parallel bogies, as used by its two predecessors at ASL: the Shrimp [11] and the SOLERO [7].

A. Suspension System

Each structure on the side is formed mainly of two parallel bogies, one between the front and the middle wheel and one between the middle and the back wheel. They are connected at the bottom next to the axis of the middle wheel and at the top through an articulated rocker. Those structures are attached on each side to the body with a simple pivot joint.

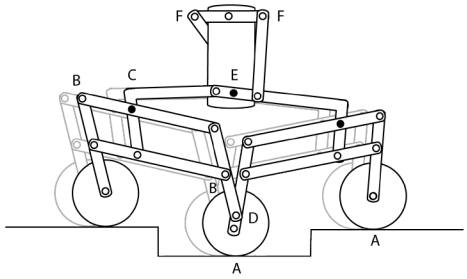

Fig. 4. Complete CRAB suspension mechanism representation.

A differential between the left and right suspension levels the pitch angle of the chassis. Apart from the six drive motors, four steering units, one for each corner wheel, allow the rover to change its heading while respecting its kinematic constraints. This is important as it influences the weight distribution within the rover. The main elements regarding the mass of the rover, as well as the most important rover dimensions are listed in table I.

TABLE I

DIMENSIONS OF THE CRAB ROVER.

Description	Value	Unit
Total Mass	44	[Kg]
Body Mass	30.5	[Kg]
Wheel Mass	1.67	[Kg]
Steering Mass	0.89	[Kg]
Length	0.844	[m]
Width	0.782	[m]
Wheel diameter	0.196	[m]

B. Model

The static model is based on the Newton-Euler formulation which states that in static state all forces and all torques are in a state of equilibrium. Using a 3D model results in static indeterminacy. The mobility of a rover should be one and can be computed with Grübler's formula [12]:

$$MO = 6 \cdot n - 5 \cdot f_1 - 4 \cdot f_2 - 3 \cdot f_3 - 2 \cdot f_4 - f_5, \quad (5)$$

where MO is the mobility of the rover, n the number of mechanical parts and f_j the number of joints of all types ($j = 1 \ldots 5$). The mobility of the CRAB, according to eq. 5, is -43 whereas it should be 1. This is due to the multiples kinematic loops in the structure and redundancy of joints that provoke static indeterminacy. Therefore, the model has to be modified in order to conform to the mathematical constraints while preserving the real behavior. Table II lists the joints, indicated in Fig. 4, that are modified to obtain a CRAB model with a mobility of one.

C. Equation System

The CRAB rover moves at relatively low speeds, between $0.05\,m \cdot s^{-1}$ and $0.1\,m \cdot s^{-1}$. Due to this, dynamics effects are considered to be negligible and a static model is sufficient. Thus, the model is based on a simple Newton-Euler formulation. In three dimensions, six equations (three forces and three torques) describe the state of a solid element. These correspond to:

$$\sum_i \vec{F}_i = \vec{0} \qquad \sum_i \vec{T}_i = \vec{0}. \quad (6)$$

Having 30 parts, the CRAB is modeled by 180 independent equations describing the static equilibrium of each body and involving 14 external ground forces (six normal forces N_i, six tangential forces R_i and two lateral forces L_i at the wheels), six motor torques and 165 internal forces. As no interest is held into the internal variables, it is possible to simplify the equation system by removing most of them and reducing the number of equations. The final equation system as the following form:

$$M_{38\times43} \cdot \vec{V}_{43\times1} = \vec{b}_{38\times1}, \quad (7)$$

where $\vec{V}$ corresponds to a vector containing the remaining forces, including the wheel ground interaction forces and wheel torques. M and $\vec{b}$ correspond to the model of the CRAB rover describing the rover state.

TABLE II

SIMPLIFICATION RESULT OF THE VARIOUS JOINTS.

Joint	Forces		DoF
	Transmitted	Free	
Pivot	$F_x\ F_y\ F_z\ T_x\ T_z$	T_y	1
Spherical	$F_x\ F_y\ F_z$	$T_x\ T_y\ T_z$	3
A	$F_x\ F_z$	$F_y\ T_x\ T_y\ T_z$	4
B	$F_x\ F_y\ F_z$	$T_x\ T_y\ T_z$	3
C	$F_x\ T_x$	$F_y\ F_z\ T_y\ T_z$	4
D	$F_x\ F_z$	$F_y\ T_x\ T_y\ T_z$	4
E	$F_x\ F_y\ F_z$	$T_x\ T_y\ T_z$	3
F	$F_x\ F_z\ T_x\ T_z$	$F_y\ T_y$	2

IV. HARDWARE

In order to implement and test the torque control algorithm on the real platform, it is necessary to get all the necessary inputs to the model. The actuator and sensory system (Fig. 5) of the CRAB rover is presented in this section and the sensors providing the needed information are described.

A. System Overview

In order to use the model presented in the previous section, the orientation of all parts of the suspension system are needed. This information can be either measured or computed based on measurements. The sensors used for this purpose are described below.

- An Inertial Measurement Unit (IMU) is mounted on the body of the CRAB. It provides the orientation (Euler angles, ψ_i with i being x and y) of the chassis.
- The angular sensors measure the relative angle of a pivot joint. Three on each side are positioned on specific joints of the mechanical structure (marked black joints in Fig. 4) providing the angles τ_i, with $i \in [1, 6]$.
- The tactile wheels provide the information about the wheel ground contact angles γ_i, with $i \in [1, 6]$. This input to the model is crucial to compute the optimal torques in uneven terrain.

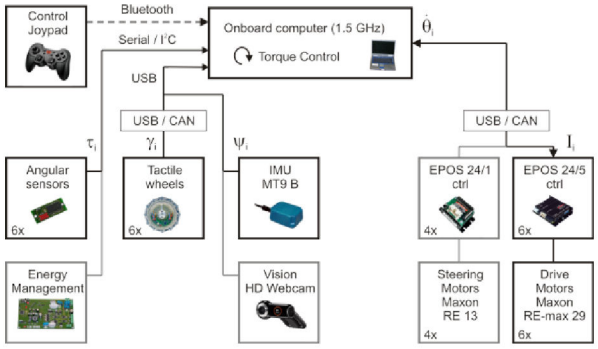

Fig. 5. Schematic of the system of the CRAB rover.

B. Implementation

M and $\vec{b}$ in eq. 7 can be computed based on the sensory input from the IMU, the angular sensors and the tactile wheels.

$$M(\psi_i, \tau_i, \gamma_i) \cdot \vec{V} = \vec{b}(\psi_i, \tau_i, \gamma_i) \tag{8}$$

Then optimizing the system based on H (eq. 3), an optimal set of torque can be computed. This is the basis to compute the correction torques to be applied to the driving motors, based on the wheels speed ($\dot{\theta}_i$).

$$T_i = K_t \cdot I_i \tag{9}$$

Eq. 9 allows determining the current to be concretely set within the motor controllers. K_t is a constant obtained from the datasheets of the motor constructor (Maxon in this case).

C. Tactile Wheels

The wheel ground contact angle is a necessary input to the system and is acquired using a home-made sensor. The goal is to use a flexible wheel and to measure the location of its maximal deformation, representing the wheel-ground contact angle.

The tactile wheel is a flexible wheel as depicted in Fig. 6, whose two basic elements, rim and ring, are made of metal. The rim is connected to the motor unit's output shaft. Spring elements transmit the torque from the rim to the flexible ring and keep the two elements at a well defined distance relative to each other. The selection of the spring elements is critical since they influence torque transmission and wheel deformation significantly. The arrangement as well as dimensions and thickness of the springs have an impact on the characteristic of the wheel. The whole design process and trade-off of different designs can be found in [13]. To transform the flexible wheel into a tactile wheel, the deformation has to be monitored and the location (angle) of its biggest amplitude has to be localized. For this purpose, infrared (IR) distance sensors, with a sub-millimeter precision, are integrated inside the wheel. Fig. 7 shows the data measured by the front left wheel of the CRAB rover climbing a step obstacle. The first 140 samples show a wheel deformation corresponding to the load previously described. The portion a corresponds to the wheel climbing the step and then the wheel is on the step. The computed wheel ground contact angle is shown in Fig. 8.

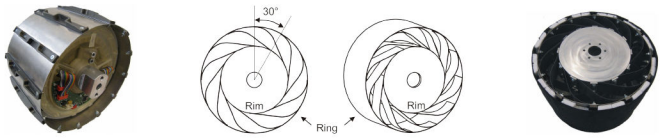

Fig. 6. On the left, the back view of the tactile wheel. In the center, a schematic showing the structure of the tactile wheel. On the right, the cover, or "sock", used for experimentations and allowing us to change of friction coefficient.

The noisy data observed can be explained by the vibration generated by the wheel rotation. As the rover is moving with a low speed, a low pass filter is used to filter the overall wheel ground contact angle.

$$y_t = \alpha \cdot x_t + (1 - \alpha) \cdot y_{t-1} \tag{10}$$

Fig. 8 shows that a clear winner can be elected among the IR sensors when the load is important (case a) whereas in case b, the reduced load on the wheel result in a reduced deformation of the wheel which is more difficult to observe. Therefore, an adaptive low-pass filter, with a coefficient evolving depending on the wheel load (difference between the smallest and the biggest distances measured) is implemented as follows:

$$\alpha = \begin{cases} 0.01 & \text{if the difference is below } 3\,mm, \\ 0.3 & \text{otherwise.} \end{cases} \tag{11}$$

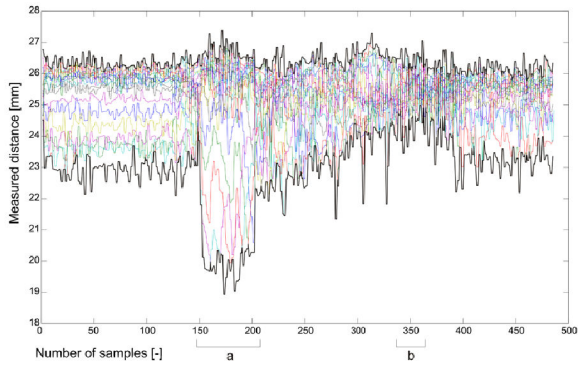

Fig. 7. IR sensors data measured during a step obstacle climb.

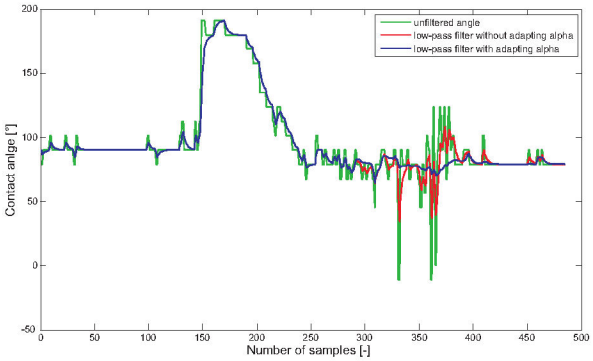

Fig. 8. Wheel ground contact angle measured during a step obstacle climb. On flat ground the measured angle is 90°. As soon as the wheel has climbed the step, the measured angle is around 80° since the bogie is rotated.

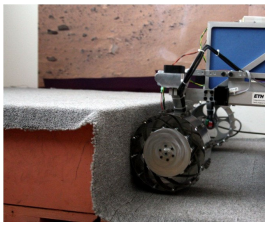

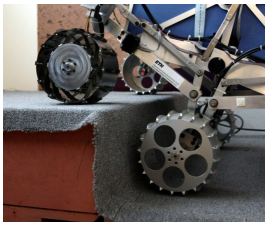

Fig. 9. Extreme load situation for the tactile wheel climbing a step. Case a on the left and b on the right.

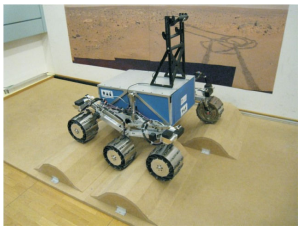

Fig. 10. CRAB evolving on the test track.

Its effect is depicted by the blue curve in the bottom graphic of Fig. 8. Note also that the position of the wheel with respect to the obstacle in both cases can be observed in Fig. 9. To summarize, the tactile wheel provides at $10\,Hz$ a wheel ground contact angle, which is required for the torque control.

V. Experimental Results

A test environment was set up to develop, test, and compare the torque control algorithm. This set up as well as the results are discussed below.

A. Setup

The test terrain has a sinusoidal shape where the left and right side are out-of-phase by $180\,^\circ$ (Fig. 10). The bumps are scaled to reach a maximum height of $0.12\,m$ which is slightly more than a wheel radius. This terrain was selected because it represents a highly uneven terrain in which good control is expected to have a major impact on the performance if conditions are difficult, i.e., if the friction coefficient is low and the wheels are likely to slip. In order to change the friction coefficient between the wheel and the ground, the wheels are covered with "socks", as depicted in Fig. 6. Thus, the friction coefficient is tuned by adding tape with different gliding properties around the wheels.

The rover is tested on the described track with the two control types, simple velocity control and the presented torque control. The tests are done with static friction coefficients μ_0 of 0.35, 0.55 and 0.75 and the speed of the rover is set to $0.1\,m \cdot s^{-1}$. The length of the test terrain is approximately $2.4\,m$. One test run consists of moving once across the track from one side to the other. Several runs (4 to 7) are done for each controller and the averaged measurements are then compared.

B. Results

The main performance criterion in this analysis is slip. This choice is motivated by the fact that several aspects of a rover mission demand for as little slip as possible. Navigation is more accurate if the rover does not slip; since slipping wheels do not contribute to the rover's movement, slip is a loss of energy; potential slip increases the risk of an operation failure due to loss of control of the vehicle.

There are two situations where slip occurs: the wheels are fighting each other due to uneven terrain or different commanded wheel velocities; the applied torque is too high and the ground cannot sustain the created traction. Torque control tries to avoid the latter by assigning bigger torques on wheels where the load is bigger because more traction can be generated. For the experiments, the slip per wheel is determined by subtracting the measured traveled distance from the encoder value of the respective motor. The traveled distance is determined by measuring the distance between start- and endpoint of the wheels. This approach to determine the slip only takes the total traveled distance into account. Local slippage, such as sliding when the wheel is moving up and down the obstacles compensates itself in the final calculation. This approach describes consistently the overall behavior and is therefore a valid measure to evaluate and compare the performance of both controllers.

In summary, the performance metrics applied for the hardware experiments are:

- Absolute slip per wheel $s_a = \lambda - d$, where d is the measured traveled distance and λ is distance based on the encoders value.
- Torque T with mean value of a full run $\overline{T}$.

The numerical results for s_a and $\overline{T}$ are given in Tables III and IV for both types of control and all friction coefficients.

C. Discussion

In terms of slippage the torque control approach performs better than velocity control in slippery conditions. For a high friction coefficient the difference between the controllers diminishes, as depicted in Fig. 11. In other words, the more traction is provided by the ground, the less important is the optimal choice of wheel torques.

The slip values suggest that the gain through torque control is limited to slippery surfaces. However, the $\overline{T}$ values point out another problem of velocity control. As depicted in Fig. 12, even in uncritical conditions, $\mu = 0.75$, $\overline{T}$ is considerably higher in velocity control mode, 1.51 Nm compared to 1.05 Nm. This is linked to the fact that the control is unsynchronized across the rover. The controller of each wheel tries to reach the commanded speed regardless of the action of the other controllers. This can lead to situations where wheels are fighting against each other, i.e., one wheel is pushing while the other one has to brake in return. In contrast, there is only one PID controller for the torque control algorithm and minimizing the error between desired and actual velocity can be regarded as a common effort. If the rover is too slow, all torques are increased; if the rover is too fast, all torques are reduced. Only the amount by which

TABLE III

RESULTS FOR METRIC s_a $[mm]$.

Control	Friction coefficient μ		
	0.75	0.55	0.35
velocity	8	45	87
torque	9	31	54

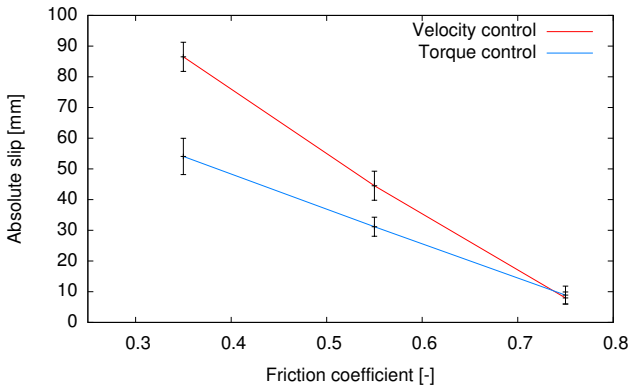

Fig. 11. Absolute slip for both controllers.

TABLE IV

RESULTS FOR METRIC $\overline{T}$ $[Nm]$.

Control	Friction coefficient μ		
	0.75	0.55	0.35
velocity	1.51	1.24	1.19
torque	1.05	0.67	0.66

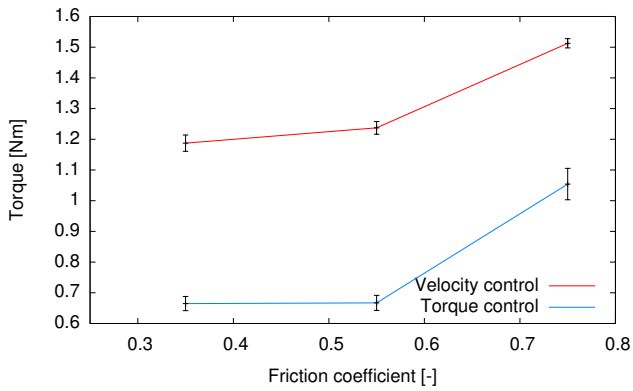

Fig. 12. Required torque for both controllers.

the torque is varied depends on the normal force on each wheel. These two distinct behaviors explain the difference in performance with respect to $\overline{T}$. Furthermore, due to the minimized slippage, no torque is wasted for unnecessary corrections of the wheels when slipping.

VI. CONCLUSION AND OUTLOOK

The implementation and the results of an enhanced controller based on an optimal torque distribution are presented in this paper. A rover model provides the basis to compute the optimal torques which minimize slip on the rover's wheels. The controller itself uses the optimally distributed torques and adds a correction term based on the rover's velocity.

The controller was implemented on a rough-terrain rover called CRAB. The hardware has to provide all the necessary information which describes the rover's state. The sensors necessary, including the tactile wheel, are presented in this paper. The tactile wheel is based on a flexible wheel whose deformation is measured to provide the wheel-ground contact angle. The controller is evaluated and compared to a standard velocity controller. It shows very good results as the torque based controller has reduced slip and torque values for all tested friction coefficients.

The next step of the work lies in the evaluation of the approach in a realistic environment. The torque control approach should lead to a better terrainability and smaller energy consumption in a real outdoor environment. Hence the model should be improved to handle the wheel sinkage as well as more complex trajectories for the rover.

ACKNOWLEDGMENTS

The authors gratefully acknowledge E. Carrasco for his work related to the design and realization of the tactile wheel, as well as F. Seitz for his contribution related to the CAN network implementation.

REFERENCES

[1] D.S. Apostolopoulos, "Analytical Configuration of Wheeled Robotic Locomotion", CMU, 2001.

[2] S.V. Sreenivasan and B.H. Wilcox, "Stability and Traction Control of an Actively Actuated Micro-Rover", *Journal of Field Robotics*, vol. 11:6, 1994.

[3] E.T. Baumgartner, H. Aghazarian and A. Trebi-Ollennu, "Rover Localization Results for the FIDO Rover", *SPIE*, vol. 4571, 2001, pp 34-44.

[4] K. Iagnemma and S. Dubowsky, "Mobile Robot Rough-Terrain Control (RTC) For Planetary Exploration",*Proceedings of the 26th ASME Biennial Mechanisms and Robotics Conference, DETC*, 2000.

[5] P. Lamon, A. Krebs, M. Lauria, R. Siegwart and S. Shooter, "Wheel torque control for a rough terrain rover", *IEEE International Conference on Robotics and Automation (ICRA)*, New Orleans, USA, 2004.

[6] P. Lamon and R. Siegwart, "Wheel torque control in rough terrain - Modeling and simulation", *IEEE International Conference on Robotics and Automation (ICRA)*, Barcelona, Spain, 2005.

[7] S. Michaud, A. Schneider, R. Bertrand, P. Lamon, R. Siegwart, M. Van Winnendael and A. Schiele, "SOLERO: Solar powered exploration rover", *7th ESA Workshop on Advanced Space Technologies for Robotics and Automation (ASTRA)*, Noordwijk, The Netherlands, 2002.

[8] A. Angelova, L. Matthies, D. Helmick and P. Perona, "Learning and Prediction of Slip from Visual Information", *Journal of Field Robotics*, vol. 24:3, 2007, pp 205-231.

[9] T. Thueer, A. Krebs, P. Lamon and R. Siegwart, "Performance Comparison of Rough-Terrain Robots - Simulation and Hardware", *Journal of Field Robotics*, vol. 24:3, 2007, pp 251-271.

[10] T. Thueer, P. Lamon, A. Krebs and R. Siegwart, "CRAB - Exploration Rover with Advanced Obstacle Negotiation Capabilities", *9th ESA Workshop on Advanced Space Technologies for Robotics and Automation (ASTRA)*, Noordwijk, The Netherlands, 2006.

[11] T. Estier, Y. Crausaz, B. Merminod, M. Lauria, R. Piguet and R. Siegwart, "An innovative space rover with extended climbing abilities", *Ecole Polytechnique Fédérale de Lausanne (EPFL)*, 2000.

[12] M. Grübler, "Getriebelehre: Eine Theorie des Zwanglaufes und der ebenen Mechanismen", Berlin, Julius Springer, 1917.

[13] A. Krebs, T. Thueer, E. Carrasco and R. Siegwart, "Towards torque control of the CRAB rover", *International Symposium on Artificial Intelligence, Robotics and Automation in Space (i-SAIRAS)*, Los Angeles, USA, 2008.